Surface marker expression in small and medium/large mesenchymal stromal cell-derived extracellular vesicles in naïve or apoptotic condition using orthogonal techniques

Renata Skovronova[1], Cristina Grange[2], Veronica Dimuccio[1], Maria Chiara Deregibus[3], Giovanni Camussi[2] and Benedetta Bussolati[1#]

[1]Department of Molecular Biotechnology and Health Sciences, University of Turin, Turin, Italy.

[2]Department of Medical Sciences, University of Turin, Turin, Italy.

[3]2i3T Business Incubator and Technology Transfer, University of Turin, Turin, Italy

Renata Skovronova: renata.skovronova@unito.it, ORCID iD: 0000-0003-0217-5309

Cristina Grange: cristina.grange@unito.it, ORCID iD: 0000-0002-6960-5476

Veronica Dimuccio: veronica.dimuccio@unito.it

Maria Chiara Deregibus: mariachiara.deregibus@unito.it

Giovanni Camussi: giovanni.camussi@unito.it, ORCID iD: 0000-0003-2795-232X

Benedetta Bussolati: benedetta.bussolati@unito.it, ORCID iD: 0000-0002-3663-5134

Word count: 4557

[#]**Correspondence**: Benedetta Bussolati, Molecular Biotechnology Centre, University of Turin, via Nizza 52, 10126 Torino, Italy. Tel. 011-6706453, Fax. 011-6631184, e-mail: benedetta.bussolati@unito.it.

Abstract

Extracellular vesicles released by mesenchymal stromal cells (MSC EVs) are a promising resource for regenerative medicine. In particular, small MSC EVs represent the active EV fraction for therapeutic applications. A bulk analysis is applied to characterize MSC EVs identity and purity, coupled with the assessment of single EV morphology, size and integrity using electron microscopy. We here applied different orthogonal methods to provide a quantitative analysis of size and surface marker expression in medium/large and small fractions, namely 10k and 100k fractions, of MSC EVs obtained by sequential ultracentrifugations. Bone marrow, adipose tissue, and umbilical cord MSC EVs were compared, in naïve and apoptotic conditions. The 100k EV size <100 nm, as detected by electron microscopy, was confirmed by super-resolution microscopy and ExoView. Quantitative single-vesicle imaging using super-resolution microscopy revealed heterogeneous patterns of tetraspanin expressions, being all MSC EV fractions single, double and triple positive, in variable proportions, for CD63, CD81 and CD9. Moreover, ExoView analysis allowed a comparative multiplex screening of single MSC EV tetraspanin and mesenchymal marker levels. Finally, a semiquantitative bead based cytofluorimetric analysis showed the segregation of immunological and pro-coagulative markers on the 10k MSC EV fraction. Apoptotic MSC EVs were released in higher number, without significant differences from the naïve fractions in surface marker expression. These results indicate that a consistent profile of MSC EV fractions among the different MSC sources, and a safer profile of the 100k MSC EV population for clinical application. Finally, our study identified suitable applications for different EV analytical techniques.

Key words: tetraspanins, 10k MSC EVs, 100k MSC EVs, Nanosight, MACSPlex, ExoView, super-resolution microscopy.

Introduction

Mesenchymal stromal cells (MSCs) are nowadays the most used cell source for regenerative medicine due to their immunomodulatory, pro-regenerative and anti-inflammatory properties (Flemming et al. 2011; Humphreys and Bonventre 2008; Bussolati et al. 2009). MSCs can originate from different tissues, including bone marrow (BM), adipose tissue (AT) and umbilical cord (UC), the ones most commonly used. As the field of extracellular vesicles (EVs) rises, so does the interest in the isolation and therapeutic application of MSC bioproducts.

Indeed, MSC EVs may overlap many of the described effects of the originating cells (Lener et al. 2015), playing an essential role in cell to cell communication, involving stem cells and target injured cells (Chargaff and West 1946; Park et al. 2019).

EVs are released from cells as a heterogeneous population that can be further classified into three fractions: small EVs, large EVs and apoptotic bodies (ApoBDs) based on their size and composition with ranges defined either as < 100 nm or < 200 nm for small EVs, and > 200 nm for medium/large EVs (Théry et al. 2018). Moreover, the classification in different EV fractions underlines distinct molecular and functional properties (Willms et al. 2016). However, small and medium/large EVs share many structural components, and a specific surface marker expression of EV fractions is lacking, due to the absence of a strict boundary between them (Yáñez-Mó et al. 2015). In particular, the classical tetraspanins, CD9, CD63 and CD81, are considered to be commonly present in different EV subpopulations (Théry et al. 2018). However, a higher expression level on small MSC EVs was reported (Bruno et al. 2017), in line with their possible origin by the cellular endosomal pathway (Théry et al. 2018). At variance, the large EV surface may more closely resemble the parental cell origin, as it can be likely associated with direct budding from the plasma membrane (Leventis and Grinstein 2010). Moreover, medium/large EVs are generally enriched with phosphatidylserine (Leventis and Grinstein 2010) and CD40 (Mobarrez et al. 2015).

The therapeutic effect of MSC EVs has been first ascribed to the entire heterogeneous EV population released by the cells under culture conditions. Subsequent studies, however, tried to identify the potentially most relevant subpopulation by fractionating MSC EVs in medium-large EVs (100-1000 nm) using a 10,000 g ultracentrifugation (10k fraction) and small MSC EVs (<100 nm) using a subsequent 100,000 g ultracentrifugation (100k fraction) and. *In vitro* and *in vivo* pre-clinical experiments clearly showed that the 100k fraction was the main responsible for functional and morphological tissue regeneration (Bruno et al. 2017; Aliotta et al. 2016; Wen et al. 2016). Indeed, the 10k and 100k fractions appeared biochemically and functionally distinct (Bruno et al. 2017; Xu et al. 2015). The small MSC EVs nowadays consider the proactive fraction retaining the therapeutic activity (Witwer et al. 2019).

The characterization of the small therapeutic MSC EVs takes into consideration the standard EV characterization, including evaluation of morphology, size and marker expression (Théry et al. 2018), coupled with the presence of typical MSC surface antigens and lack of non-MSCs markers, reflecting the identity criteria defined for the originating cells by the International Society for Cell & Gene Therapy minimal criteria (Gimona et al. 2021; Witwer et al. 2019). Indeed, it is of interest and of potential relevance for clinical application to determine and

quantify the expression of identity markers such as tetraspanins and mesenchymal markers, as well as of other immunological and pro-coagulative surface markers within the small MSC EV population as compared with medium/large EVs in MSCs of different origin.

Besides, recent studies identify that the MSC-mediated immunomodulatory effects *in vivo* are due to apoptosis, suggesting a therapeutic role for apoptotic EVs (Caruso and Poon 2018). However, knowledge of the differences between apoptotic and naïve MSC EVs is still limited. In the present work, we aimed to determine the surface marker expression of small MSC EVs isolated by sequential ultracentrifugation at 100,000 g (after removal of the 10,000 g centrifugation), and here defined as 100k MSC EVs, as compared to medium-large MSC EVs isolated at 10,000 g, and defined as 10k MSC EVs, using complementary techniques as ExoView, super-resolution microscopy and bead-based cytofluorimetric analysis. Various MSC sources of clinical interest were used, and naïve and apoptotic conditions were applied.

Material and methods

Cell cultures

The MSCs were obtained as a collaboration within the RenalToolBox ITN (Grant Agreement813839). BM-MSCs were obtained from the group of Prof. Timothy O'Brien (National University of Galway, Ireland), AT-MSCs from lipoaspirate adipose tissue processed by the group of Prof. Karen Bieback (University of Heidelberg) and UC-MSCs from the group of Dr. Jon Smythe (NHS Blood and Transplant, Liverpool, UK) from three different healthy donors with informed consent obtained in accordance with Declaration of Helsinki. MSCs were cultured and expanded under standardised protocol among the groups. In particular, all MSCs were cultured using AlphaMEM with UltraGlutamine (BE02-002F, Lonza) and 10% Foetal Bovine Serum (10270-106, Gibco) in the incubator at 37°C with 5% CO_2 and controlled humidity. MSCs were checked for the expression of mesenchymal markers by cytofluorimetric analysis (data not shown). EVs were collected from MSCs at 4-6th passage.

EV isolation

When the cells reached 80% confluency, they were starved overnight (16h) in RPMI medium (Fig.1). The supernatant was collected and centrifuged for 10min at 300 g to remove cell debris, on the second day. In experiments using apoptotic MSCs, the supernatant was transferred into new tubes and centrifuged 3000 g for 20min to collect apoptotic bodies. The supernatant was then ultracentrifuged for 1h at 10,000 g, 4°C, using the Beckman Coulter Optima L-100K Ultracentrifuge with the rotor type 70 Ti. At this speed, the subpopulation of 10k EVs was collected. The supernatant was further ultracentrifuged for 1h at 100,000 g, 4°C to obtain the 100k EV subpopulation. The EV pellet was resuspended in RPMI supplemented with 0.1% DMSO. The EV suspension was then stored at -80°C until further use.

Apoptotic vesicles were isolated from MSCs undergoing apoptosis for 24h using 500ng/ml of an Anti-Fas Ab (3510771, Merck) diluted in RPMI medium. Isolation of the apoptotic EVs followed the same ultracentrifugation protocol of the naïve MSC EVs. The ApoBDs were resuspended in RPMI supplemented with 1% DMSO.

Nanoparticle tracking analysis

After the isolation, the concentration of all the samples was measured by Nanosight NS300 (Malvern Instruments Ltd., Malvern, UK) equipped with a 488 nm laser module that utilises Brownian motion and refraction index. The particle size scatters 10 nm to 1000 nm, although

the optimised size range is 70 - 300 nm. It uses the scattered light to detect a particle and tracks its motion as a function of time. The particles' scattered light was recorded with a light-sensitive camera under 90° angle to the irradiation plane. This angle allows the Brownian motion of the EVs. Samples were diluted 1:100 in Milli-Q H_2O. For each sample, 3 videos of 60sec at camera level 15 and threshold 5 were captured using a syringe pump 30. All the samples were characterised with NTA 3.2 Analytical software. The NTA settings were kept constant between samples.

Transmission electron microscopy

The transmission electron microscopy (TEM) was performed on EVs placed on 200-mesh nickel formvar carbon-coated grids (Electron Microscopy Science) for 20min to promote adhesion. The grids were then incubated with 2.5% glutaraldehyde plus 2% sucrose. EVs were negatively stained with NanoVan (Nanoprobes, Yaphank, NY, USA) and observed using a Jeol JEM 1400 Flash electron microscope (Jeol, Tokyo, Japan).

Cytofluorimetric analysis

MACSPlex Exosome Kit (Miltenyi Biotec, Bergisch Gladbach, Germany) containing fluorescently labelled capture beads coupled to 37 exosomal surface epitopes and 2 isotope controls was used, following the manufacturer's instructions. Briefly, 15 µl of beads were added to 120 µl of buffer or sample, including a total of $1x10^9$ EVs and the complex was then incubated on a rotor overnight at 4°C. After the incubation and washing steps, a cocktail of APC fluorescent antibodies against tetraspanins were added and set on the rotor for 1h at room temperature. After washing, samples were detected using BD FACSCelesta™ Flow Cytometer (BD Bioscience, NJ, USA). Median background values of buffer control were subtracted, and samples were normalised to the mean fluorescence intensity of tetraspanins.

ExoView chip-based analysis

NanoView Biosciences (Boston, MA, USA) customised silicone chips coated with tetraspanins, CD44 and CD105 were incubated overnight with $1x10^8$ MSC EVs suspension diluted in a final volume of 35 µl of incubation buffer A, at room temperature. After the incubation, chips were washed 3 times for 3min on an orbital plate shaker with wash solution B. The chips were scanned with the ExoView™ R100 reader (NanoView Biosciences) by the ExoScanner software. The particle size scatters 50 nm to 200 nm. The data were analysed using ExoViewer software. The number of captured EVs for each surface epitope were compared between the samples.

Super-resolution microscopy

Super-resolution microscopy pictures of EVs were obtained using a temperature-controlled Nanoimager S Mark II microscope from ONI (Oxford Nanoimaging, Oxford, UK) equipped with a 100x, 1.4NA oil immersion objective, an XYZ closed-loop piezo 736 stage, and 405 nm/150 mW, 473 nm/1 W, 560 nm/1 W, 640 nm/1 W lasers and dual/triple emission channels split at 640 / and 555 nm. The samples were prepared using 10 µl of 0.01% Poly-L-Lysine (Sigma-Aldrich, St. Louis, MO, USA) placed on high- precision coverslips cleaned in sonication bath 2 times in dH_2O and once in KOH, in silicon gasket (Sigma-Aldrich, St. Louis, MO, USA). The coated coverslips were placed at 37 °C in a humidifying chamber for 2h. Excess of Poly-L-Lysine was removed. 1 µl of EVs ($1x10^{10}$) resuspended in 9 µl of blocking solution (PBS-5% Bovine Serum Albumin) were pipetted into a previously coated well to attach overnight at +4 °C. The next day, the sample was removed, and 10 µl of blocking solution was added into the wells for 30min. Antibodies were directly conjugated as follows:

2.5 µg of purified mouse anti-CD9 was conjugated with Atto 488 dye (ONI, Oxford, UK), anti-CD63, CD40 and Annexin V antibodies (Santa Cruz: SC-5275, SC-13128, SC-8300) were conjugated with Alexa Fluor 555 dye. Anti-CD81, Annexin A1 and Anti-Phosphatidylserine antibodies (Santa Cruz; SC-31234, SC-12740, Merk 05-719) were conjugated with Alexa Fluor 647 dye using the Apex Antibody Labelling Kit (Invitrogen, Carlsbad, CA, USA) according to the manufacturer's protocol. Samples were incubated with 1 µl of each antibody, added into blocking buffer at a final dilution 1:10, under light protection, overnight at +4 °C. The day after, samples were washed twice with PBS, and 10 µl of the mixed ONI B-Cubed Imaging Buffer (Alfatest, Roma, Italy) was added for amplifying the EV imaging. Two-channel (647 and 555) dSTORM data (5000 frames per channel) or three channels (2000 frames per channel) (647, 555 and 488) were acquired sequentially at 30 Hertz in total reflection fluorescence (TIRF) mode. Before each imaging session, beads slide calibration was performed to align fluorescent channels, achieving a channel mapping precision smaller than 12 nm. Single-molecule data was filtered using NimOS (Version 1.18.3, ONI) based on the point spread function shape, photon count and localisation precision to minimise background noise and remove low-precision and non-specific co-localisation. All pictures were analysed using algorithms developed by ONI via their CODI website platform (https://alto.codi.bio/). The filtering and drift correction was used as in NimOS software. The BDScan clustering tool was applied to merged channels, and co-localised EVs were also counted in separate channels.

Statistical Analysis

Data are shown as mean ± SD. At least three independent replicates were performed for each experiment. Statistical analysis was carried out on Graph Pad Prism version 8.04 (GraphPad Software, Inc, San Diego, CA, USA) by using the two-way ANOVA followed by Turkey's multiple comparisons test, where appropriate. A p value < 0.05 was considered significant.

Results

Isolation of 100k and 10k MSC EVs and size analysis

Two MSC EV fractions were isolated by sequential centrifugations, as detailed in Methods: in particular, medium/large MSC EVs were isolated by a 10,000 g ultracentrifugation (10k fraction), followed by the small MSC EV isolation from the remaining supernatant by a 100,000 g ultracentrifugation (100k fraction) (Fig.1). MSCs were obtained from bone marrow, adipose tissue and umbilical cord, from three different donors for each cell source. To allow comparison among MSC EVs of different origin, we cultured MSCs in standardized superimposable conditions.

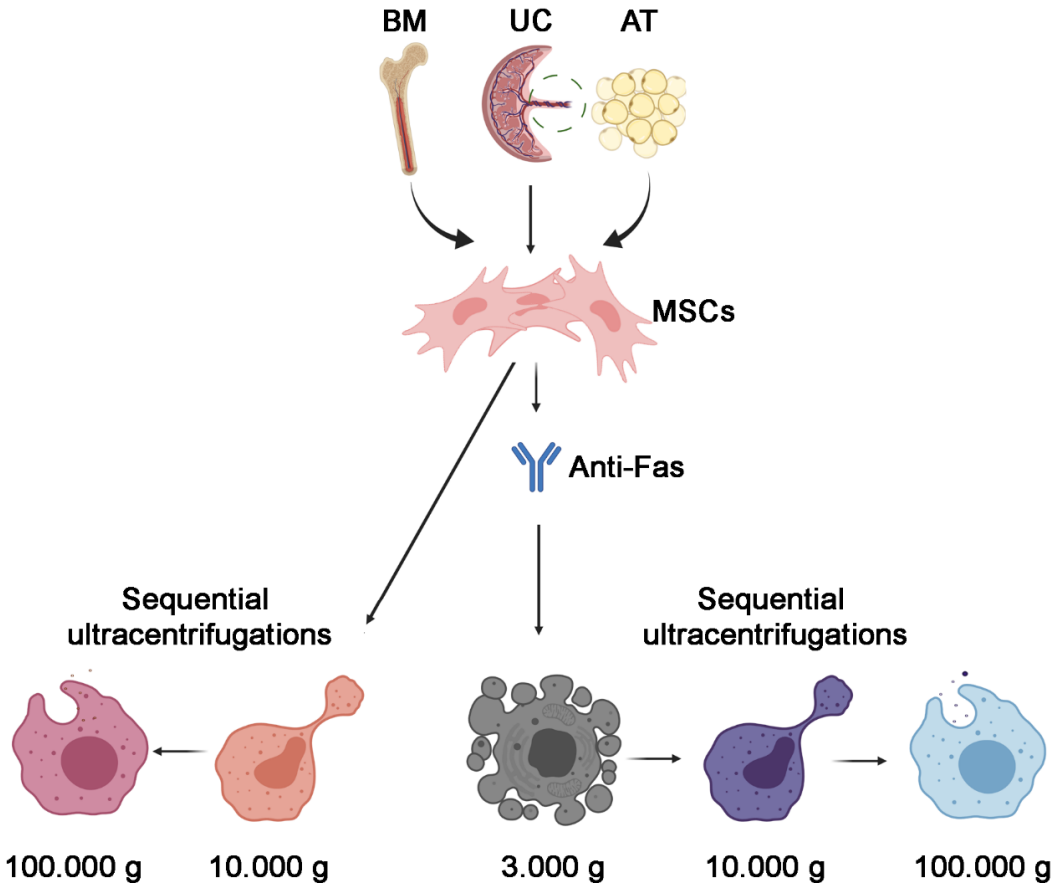

Figure 1: Scheme of different EV fractions used in this study. Naïve and apoptotic MSC EVs, induced with anti-Fas antibody, obtained from bone marrow (BM), umbilical cord (UC) or adipose tissue (AT) were isolated using subsequent differential ultracentrifugations.

The 100k and 10k MSC EV fractions were first analysed using Nanoparticle tracking analysis (Fig. 2A), that confirmed 100k MSC EVs as a homogenous population. At variance, 10k EVs

showed a multi-peak profile, indicating the presence of fractions with a highly variable size (Fig. 2A). Transmission electron microscopy analysis showed the 100k EV morphology, as spherical, membrane-encapsulated particles with a characteristic cup-shaped aspect (Fig. 2B). In contrast, the 10k EVs represented a heterogeneous population of EVs, differing greatly in size, shape, and electron-density (Fig. 2B). Quantitative size analysis using Nanoparticle tracking analysis showed that EV size (mode size) was superimposable between the different MSC EV sources (Table 1).

Table 1: Average size and EVs concentration in 1 ml measured by Nanosight.

	100k				10k			
Naïve	Mode (nm)	SD	Concentration (particles/ml)	SD	Mode (nm)	SD	Concentration (particles/ml)	SD
BM	187.70	14.31	5.1×10^8	2.4×10^8	188.83	2.73	5.8×10^8	3.1×10^8
UC	184.23	19.63	3.6×10^8	2.1×10^8	197.07	8.54	6.8×10^8	4.9×10^8
AT	208.53	26.44	6.2×10^8	2.5×10^8	238.61	25.38	6.2×10^8	2.7×10^8

	100k				10k			
Apoptotic	Mode (nm)	SD	Concentration (particles/ml)	SD	Mode (nm)	SD	Concentration (particles/ml)	SD
BM	183.67	15.63	1.4×10^9	1.1×10^9	169.10	18.71	1.4×10^9	1.1×10^9
UC	179.57	16.24	7.8×10^9	9.0×10^9	211.03	14.61	1.2×10^9	1.4×10^9
AT	170.90	35.94	1.1×10^9	6.7×10^8	202.77	22.80	7.9×10^9	1.0×10^9

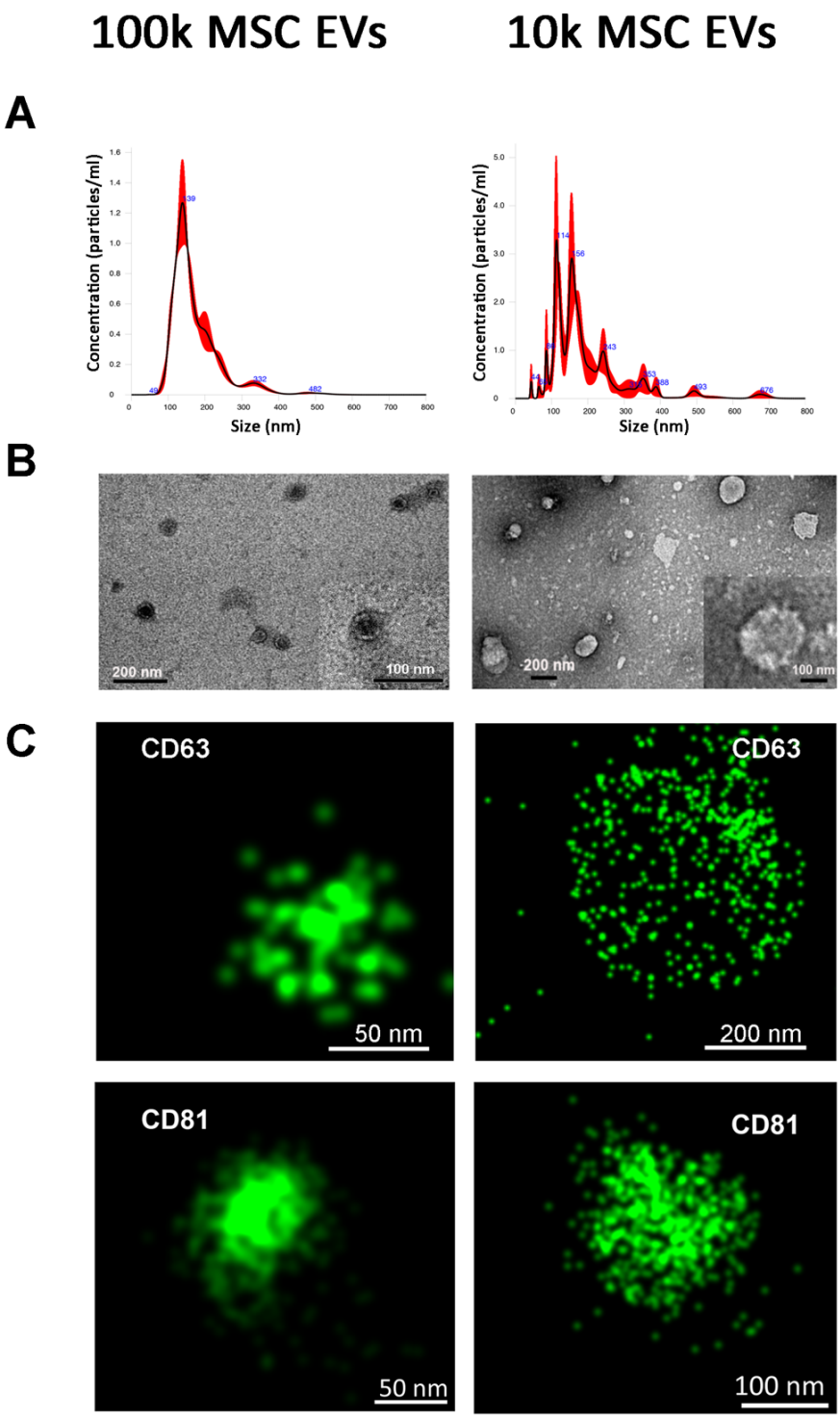

Figure 2: Characterization of 100k and 10k naïve MSC EVs. (A) Representative graphs of nanoparticle tracking analysis of 100k MSC EVs (left panel) and 10k MSC EVs (right panel). (B) Representative images of transmission electron microscopy of 100k MSC EVs (left panel) and 10k MSC EVs. The corresponding scale bare is bellow each EV image. (C) Representative super-resolution microscopy images of 100k MSC EVs (left panel) and 10k MSC EVs (right panel) stained with CD63 or CD81 tetraspanins.

In addition, no differences were detected using this technique in the size of the 100k EVs in respect to the 10k EV fractions. In contrast, by electron microscopy, the majority of 100k EVs was smaller than 100 nm, whereas the majority of 10k EVs was in a size range of 100-300 nm (Table 2).

Table 2: Mean size of EVs measured by Transmission electron microscopy, super-resolution microscopy, and ExoView.

	Sample	TEM	Super- resolution microscopy	ExoView (50-200 nm detection)
SIZE 100k EV [nm]	BM	<100	88.00 ±7.94	61.85 ±3.64
	UC	<100	88.00 ±3.46	59.14 ±2.03
	AT	<100	98.00 ±2.11	59.92 ±2.72
SIZE 10k EVs [nm]	BM	100-300	140.00 ±5.77	90.00 ±1.73
	UC	100-300	120.00 ±5.77	90.33 ±2.34
	AT	100-300	120.00 ±8.42	92.83 ±5.08

Using super-resolution microscopy based on tetraspanin staining (CD63 and CD81) on intact unfixed MSC EVs, we also confirmed the size of tetraspanin-expressing EV fractions (Fig. 2C), being 100k EVs quantified, using an automatic size analysis software, as around 90 nm median size for all MSC sources, whereas 10k EVs as around 130 nm median size (see Table 2). Single molecule analysis of CD63 expression also indicated its differential distribution on the EV surface, as 10k EVs showed a discrete surface expression, whereas 100k EVs showed a more condensed tetraspanin localization possibly due to the small size (Fig. 2C). The patchy distribution of tetraspanins was more evident on larger EVs within the 10k fraction (>500nm) (Supplementary Fig. 1).

Variable tetraspanin expression on 100k and 10k single MSC EVs by super-resolution microscopy

Transmembrane tetraspanin proteins CD63, CD9 and CD81 are a major class of EV-expressed molecules, previously reported to be enriched in 100k in respect to 10k EV fraction (Crescitelli et al. 2013; Kowal et al. 2016). We first took advantage of super-resolution microscopy to assess tetraspanin co-expression at a single EV level on 100k and 10k MSC EVs (Figure 3). Advanced three colour staining was performed using the anti-tetraspanin Abs dyed in red

(CD81), green (CD63) and blue (CD9) using dSTORM single-molecule analysis with super-resolution microscopy. Tetraspanin single-molecule surface analysis highlighted an uneven tetraspanins distribution on the EV surface. Moreover, we observed a heterogeneous tetraspanin distribution, being EVs variably positive for single, double, or triple tetraspanins (Fig. 3). We also took advantage of an automated software analysis for the quantification of the tetraspanin co-expression on single EVs (Fig. 3C, D).

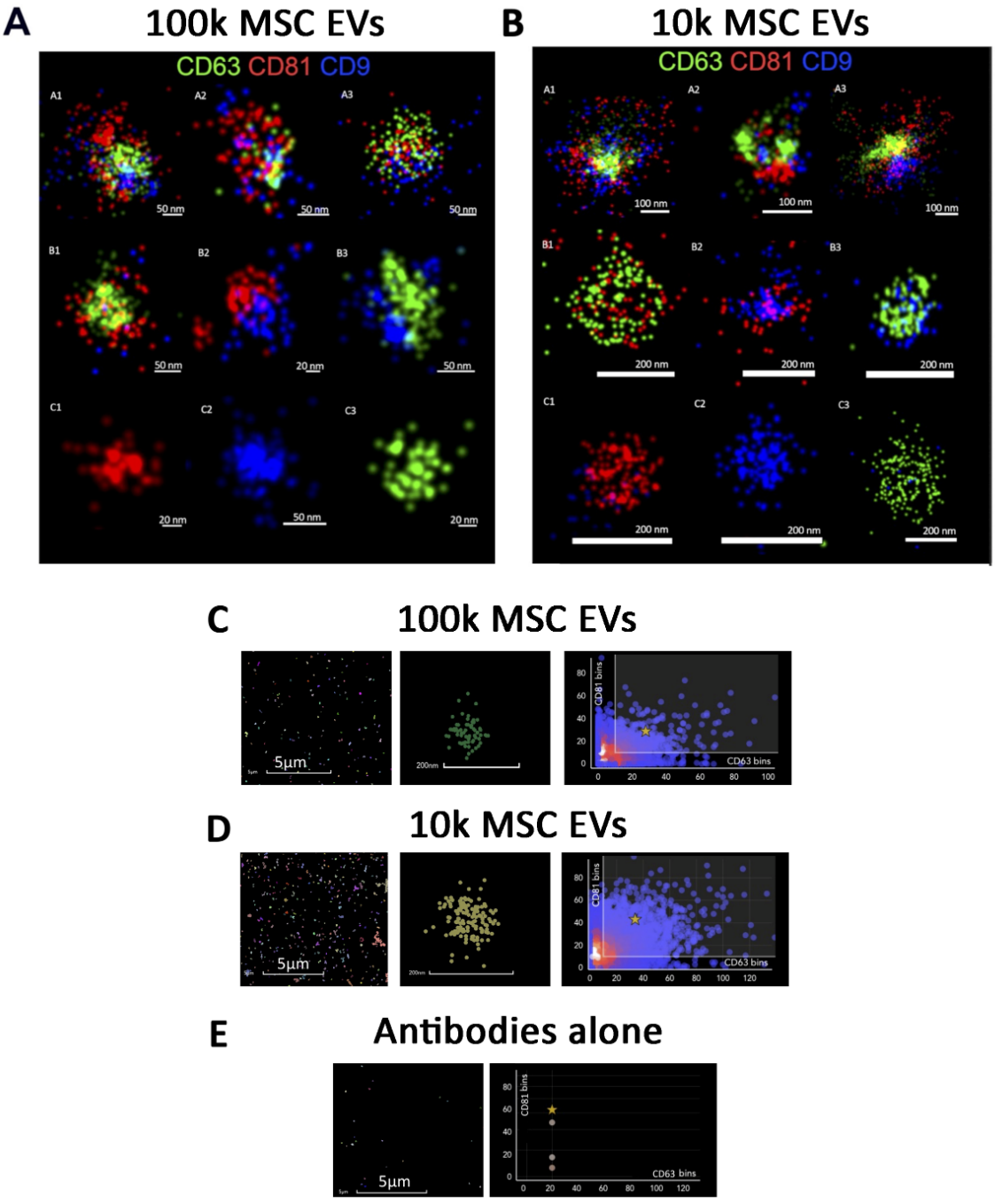

Figure 3: Super-resolution microscopy images. Representative super-resolution microscopy images of 100k EVs (A) and 10k EVs (B) stained with tetraspanins: CD81 red, CD63 green,

CD9 blue. Both panels (A, B) show triple positive, double positive and single positive MSC EVs. The corresponding scale bare is bellow each EV image. (D) Representative clustering strategy of MSC 100k EVs with large field of view (left panel), a selected cluster (central panel) and graph (right panel) showing CD81/CD63 cluster distribution. (E) Representative clustering strategy of MSC 10k EVs with large field of view (left panel), a selected cluster (central panel) and graph (right panel) showing the proportion of CD81 and CD63 antibodies/cluster. (F) Representative clustering strategy of negative control using antibodies alone without EVs showing large field of view and graph demonstrating the proportion of CD81 and CD63 antibodies.

In particular, the triple tetraspanin expression only represented a fraction of the entire EV population, being the other EVs variably positive for the different markers (Fig. 4). The 100k MSC EV fraction, in general, did not show increased tetraspanin expression in respect to the 10k fraction. CD63 was the most expressed marker in the single positive EV population in AT- and UC-MSC EVs, but not in BM-MSC EVs (Fig. 4). The 10k fraction of UC-MSC EVs showed the largest population of EVs co-expressing CD81, CD63 and CD9 (Fig. 4B). These results show a variable co-expression of the tetraspanins on MSC EV sources, without significant differences in the 10k and 100k fractions.

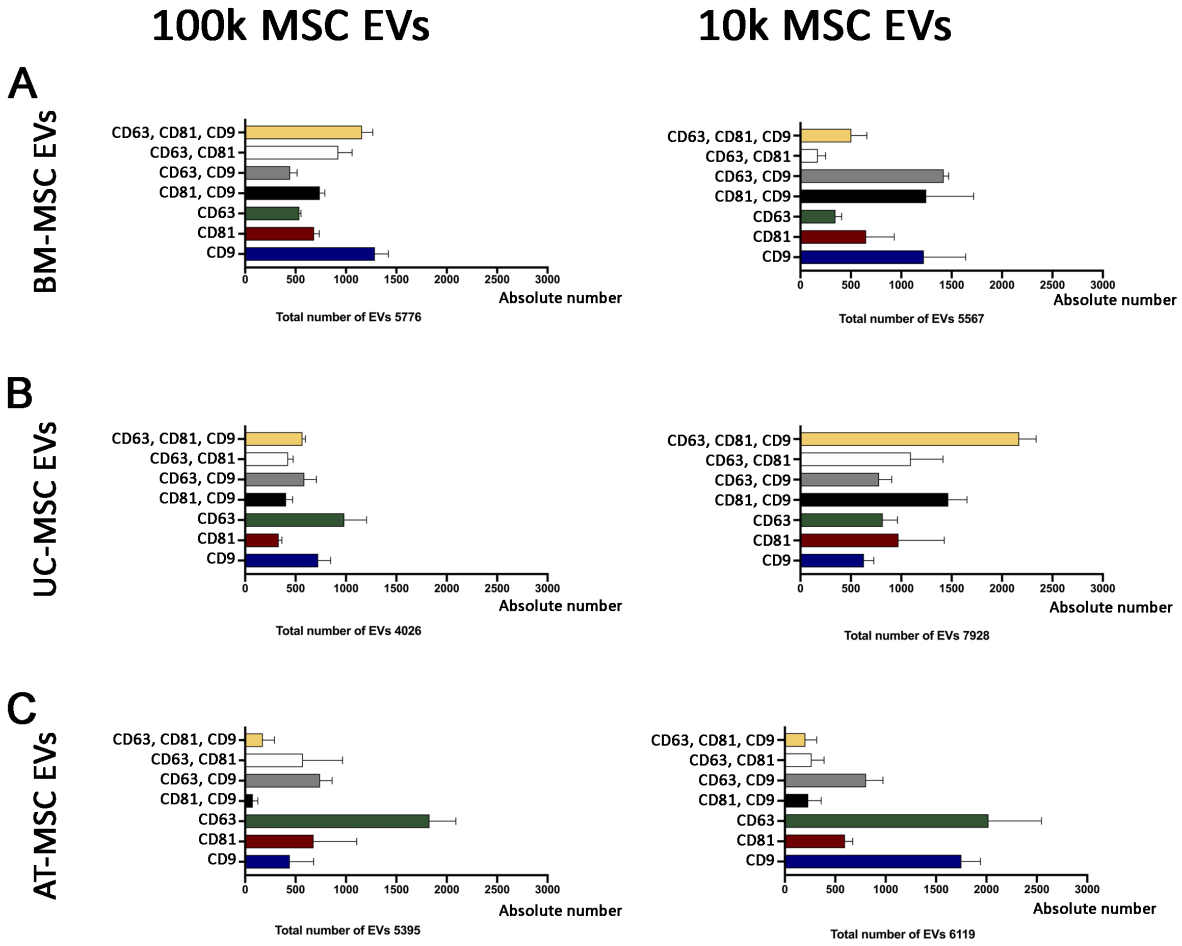

Figure 4: Super-resolution microscopy analysis of 100k and 10k MSC EVs. The graphs show triple positive, double positive and single positive EVs of 100k and 10k MSC EVs. (A) BM-MSC EVs, (B) UC-MSC EVs, (C) AT-MSC EVs. The total number of single EV analyzed is reported below each graph.

Isolation of 100k and 10k MSC EVs from apoptotic cells

We also generated 100k and 10k EVs from MSCs undergoing apoptosis using an anti-Fas Ab, as described (Adachi et al. 2003; Wang et al. 2017), for further comparison with the naïve fractions. Fas triggered MSC apoptosis induction was confirmed by Annexin V staining (Supplementary Fig. 2 and Supplementary Table 1). Moreover, apoptosis induction was also assessed by the generation of large apoptotic bodies (size range 1-5 µm), showing positivity for the apoptotic marker Annexin V by flow cytometry and by super-resolution microscopy (Supplementary Fig. 2). Moreover, apoptotic bodies also showed positivity for Phosphatidylserine (Supplementary Fig. 2C), as previously described (Tixeira et al. 2017).

Size and number of apoptotic MSC EVs were analysed by nanoparticle tracking analysis and by electron microscopy, showing similar size of the naïve MSC EVs for both 100k and 10k fractions (Table 1 and Fig. 5). However, apoptotic 100k EVs showed a less homogeneous profile than the naïve ones, by nanoparticle tracking analysis (Fig. 5A). Interestingly, the average concentration of both 100k and 10k EVs from apoptotic cells was significantly higher than that obtained from naïve cells using the same originating cell number (Table 1). Superimposable results were obtained for the three MSC sources. Using super-resolution microscopy, we detected the expression of Phosphatidylserine and Annexin V on apoptotic 100k and 10k and not on naïve MSC EVs, confirming that these markers are able to specifically characterize the apoptotic EVs (Fig. 5C, D) (Tixeira et al. 2017).

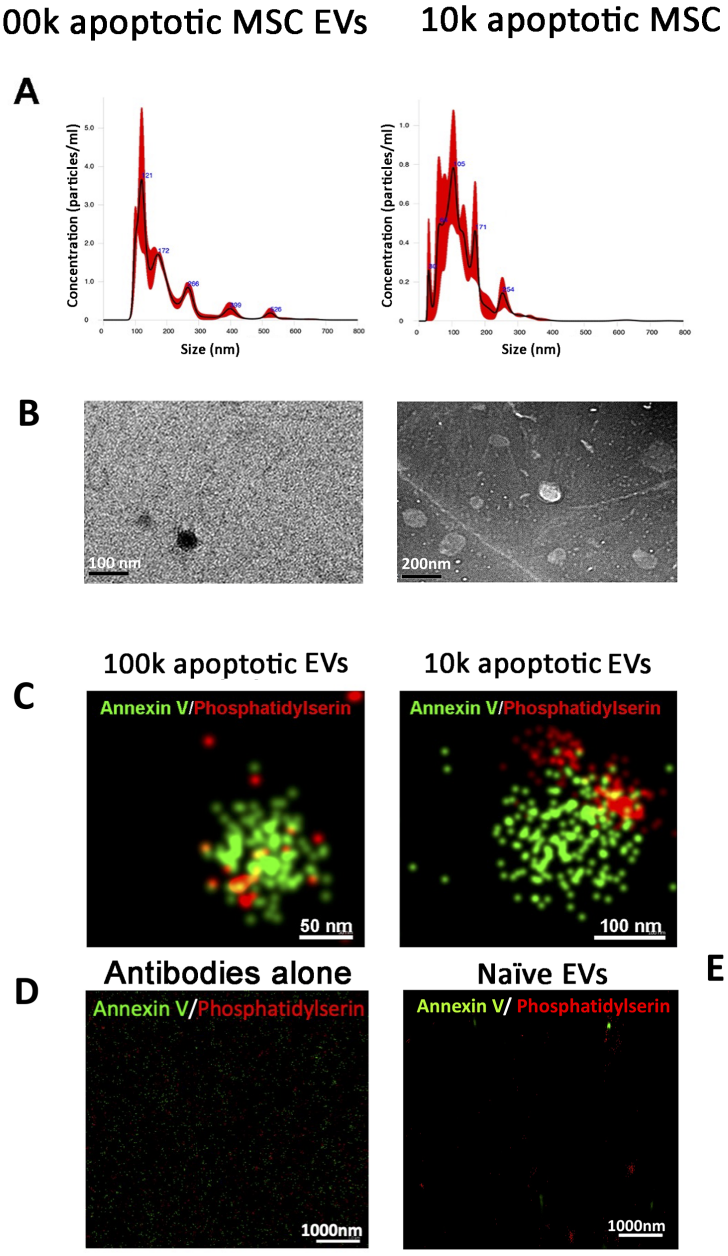

Figure 5: Characterization of 100k and 10k apoptotic MSC EVs. (A) Representative graphs of nanoparticle tracking analysis of 100k apoptotic MSC EVs (left panel) and 10k apoptotic MSC EVs (right panel). (B) Representative images of transmission electron microscopy of 100k apoptotic MSC EVs (left panel) and 10k apoptotic MSC EVs (right panel). (C) Representative super-resolution microscopy images of 100k apoptotic MSC EVs (left panel) and 10k apoptotic MSC EVs (right panel) stained with Annexin V (green) and Phosphatidylserine (red). (D) Representative super-resolution microscopy image of Annexin V (green) and Phosphatidylserine (red) as a negative control without EVs. (E) Representative super-resolution microscopy image of 100k MSC EVs isolated from naïve MSCs and stained with Annexin V (green) and Phosphatidylserine (red).

Quantitative tetraspanin evaluation of naïve and apoptotic 100k and 10k MSC EVs

We, therefore, used cytofluorimetric analysis and ExoView to gain quantitative results for comparison of tetraspanin level expression in MSC EV fractions from all different sources, in naïve and apoptotic MSC EVs.

Semiquantitative analysis of tetraspanin levels in all MSC EV subsets was performed using the MACSPlex exosome kit, a bead-based cytofluorimetric analysis. This technique did not detect differences among MSC sources, MSC EV fractions and naïve or apoptotic conditions (Fig. 6).

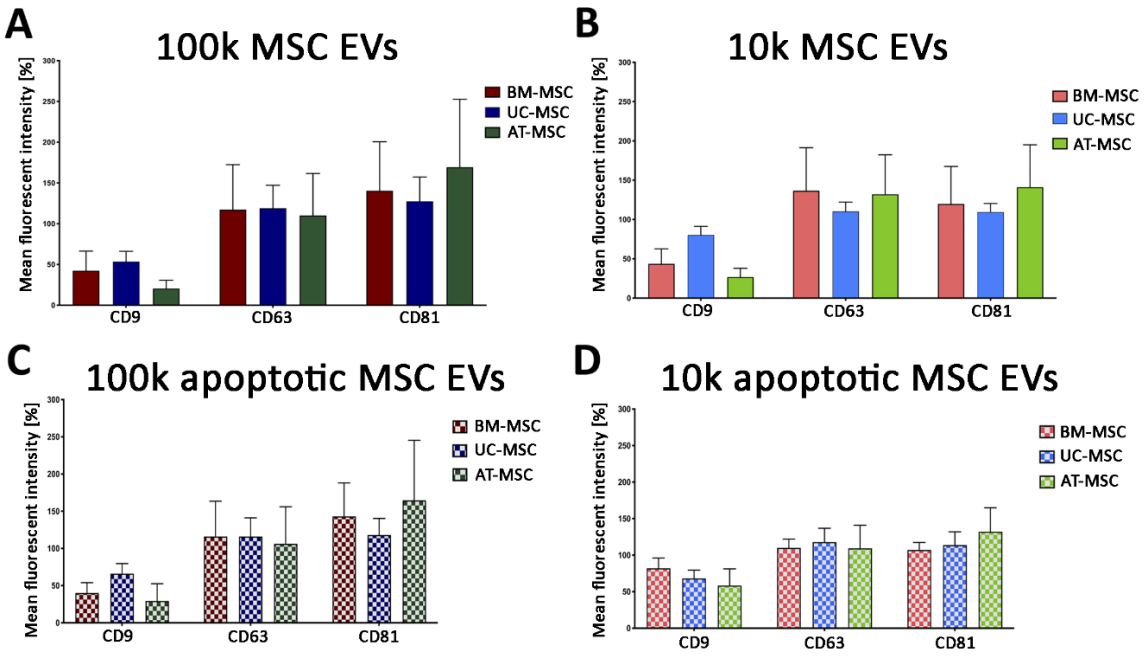

Figure 6: MACSPlex tetraspanin analysis of 100k MSC EVs and 10k MSC EVs of naïve and apoptotic MSCs. Histograms represent the mean fluorescence intensity of CD9, CD63 and CD81 tetraspanins for 100k MSC EVs (A, C) and 10k MSC EVs (B, D) isolated from naïve (A, B) and apoptotic (C, D) MSCs. BM-MSC EVs, UC-MSC EVs and AT-MSC EVs were compared. Data are expressed as mean ± SD of three different experiments.

ExoView chip-based analysis was then used to obtain an evaluation of the number of the particles captured on a specific chip coated with tetraspanins and negative mouse IgG control (MIgG). The number of EVs loaded onto each chip was normalised based on their concentration evaluated by nanoparticle tracking analysis. The results showed that the apoptotic EV fractions showed a higher number of tetraspanin-captured EVs than the naïve ones, and that the 10k fractions showed a higher number of tetraspanin-captured EVs than the 100k fractions, for all MSC sources used (Fig. 7). Among the different sources the tetraspanin

levels were significantly different, with UC-MSC EVs having the highest expression of most markers (Fig. 7).

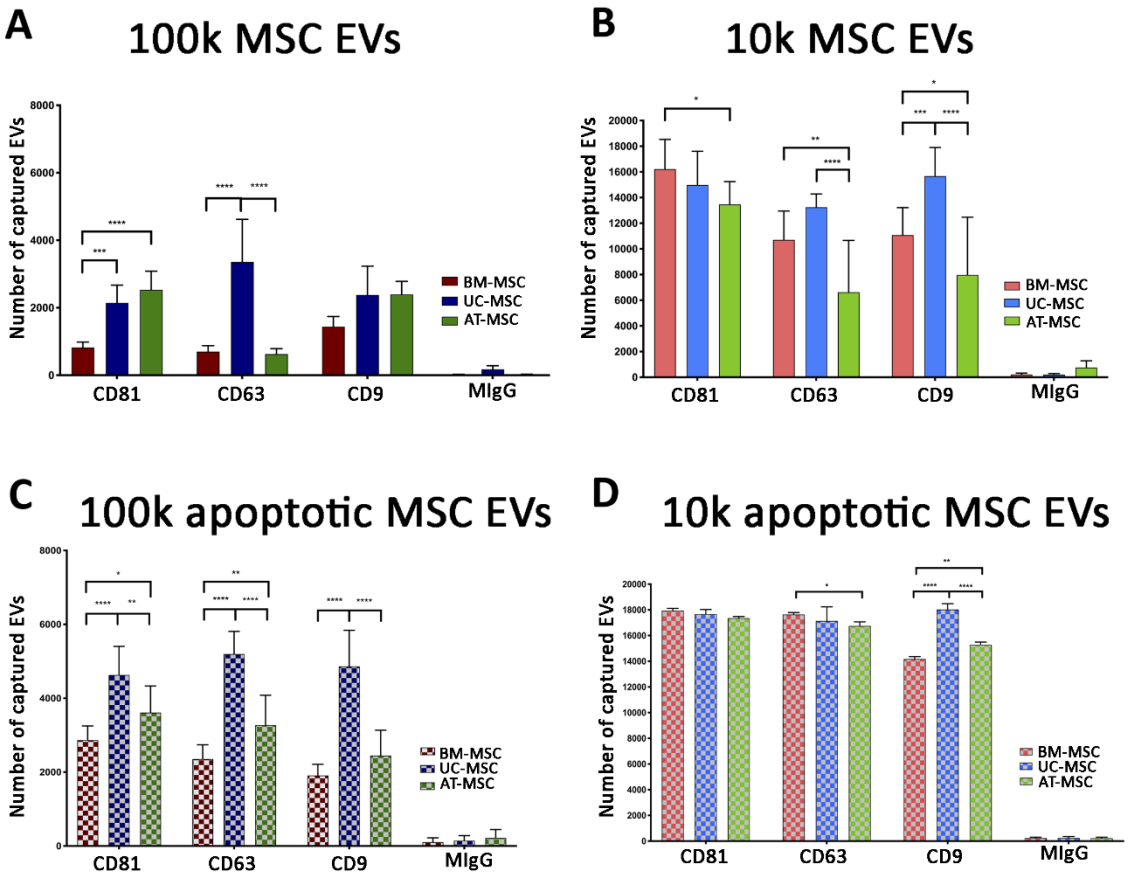

Figure 7: ExoView tetraspani analysis of 100k and 10k MSC EVs of naïve and apoptotic MSCs. Histograms represent the number of captured EVs for CD9, CD63 and CD81 tetraspanins and negative control. 100k MSC EVs (A, C) and 10k MSC EVs (B, D) isolated from naïve (A, B) and apoptotic (C, D) MSCs were analyzed. BM-MSC EVs, UC-MSC EVs and AT-MSC EVs were compared. Data are expressed as mean ± SD of three different experiments. A p value < 0.05 was considered significant (*<0.05, **<0.001, ***<0.001, ****<0.0001).

Comparing different techniques CD9 expression by MACSPlex appeared lower than other tetraspanins for all MSC sources and fractions, at variance of the results obtained using ExoView or super-resolution microscopy. These data highlight that ExoView provides a better quantitative analysis in respect to the bead-based cytofluorimetric assay, performing a semiquantitative analysis. Moreover, different antibody affinity could be present.

Mesenchymal, and immunological marker expression on naïve and apoptotic 100k and 10k MSC EVs

Mesenchymal markers are usually assessed to characterize MSC EVs (Giebel, Kordelas, and Börger 2017). MACSPlex exosome kit allowed the evaluation of CD56, CD44, CD29, CD49e, CD146 and CD105 mesenchymal marker expression on all EV fractions, from the three MSC sources in naïve and apoptotic conditions (Fig. 8).

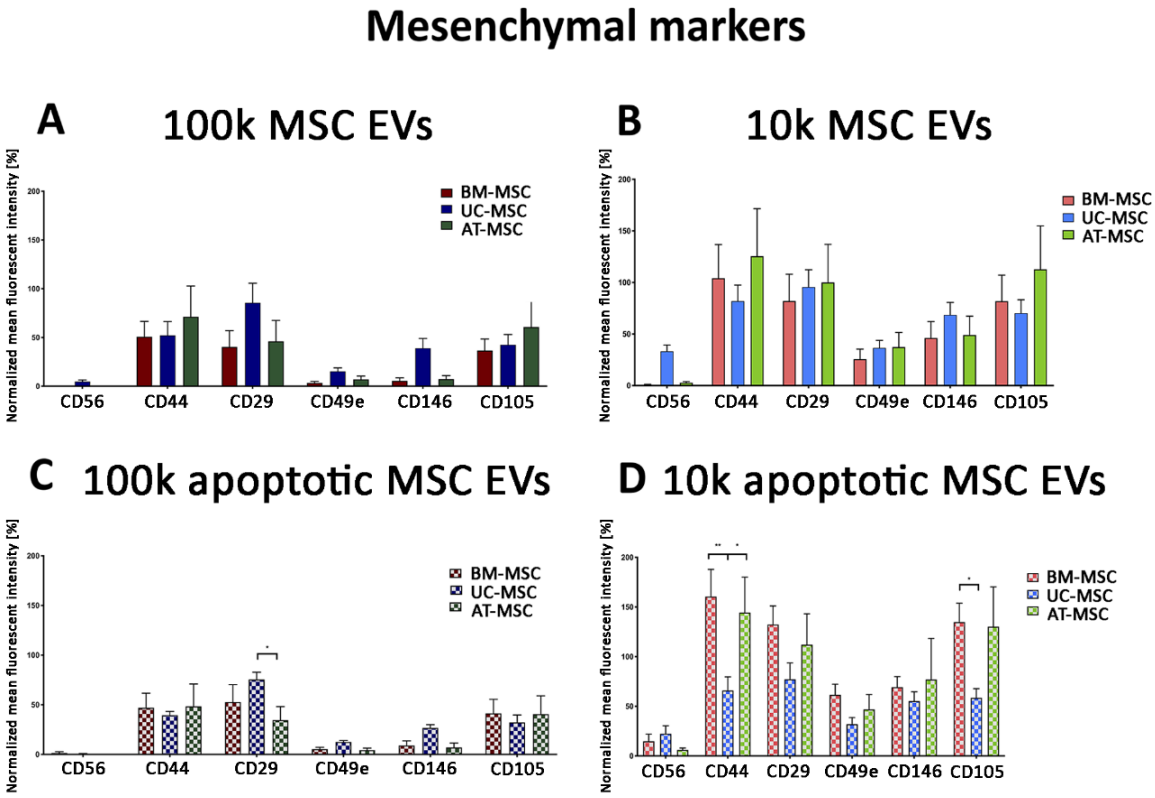

Figure 8: MACSPlex mesenchymal marker analysis of 100k and 10k MSC EVs of naïve and apoptotic MSCs. (A-D) Histograms represent normalized fluorescence intensity of mesenchymal markers (CD56, CD44, CD29, CD49e, CD146, CD105) for 100k MSC EVs (A, C) and 10k MSC EVs (B, D) isolated from naïve (A, B) and apoptotic (C, D) MSCs. BM-MSC EVs, UC-MSC EVs and AT-MSC EVs were compared. Data are expressed as mean fluorescence intensity normalized to the mean fluorescence intensity of tetraspanins± SD of three different experiments. A p value < 0.05 was considered significant (*<0.05, **<0.001, ***<0.001, ****<0.0001).

Mesenchymal markers were expressed from all MSC sources and MSC EV fractions, in the naïve and apoptotic EV conditions, but higher levels were generally observed in the 10k fraction in respect to the 100k fraction. We confirmed the expression of the mesenchymal CD105 and CD44 markers on the 100k naïve and apoptotic MSC EVs (Fig. 9A, B). CD44 and CD105 had a wider size range by size distribution of captured EVs, especially more evident in the 100k apoptotic MSC EVs (Fig. 9C, D).

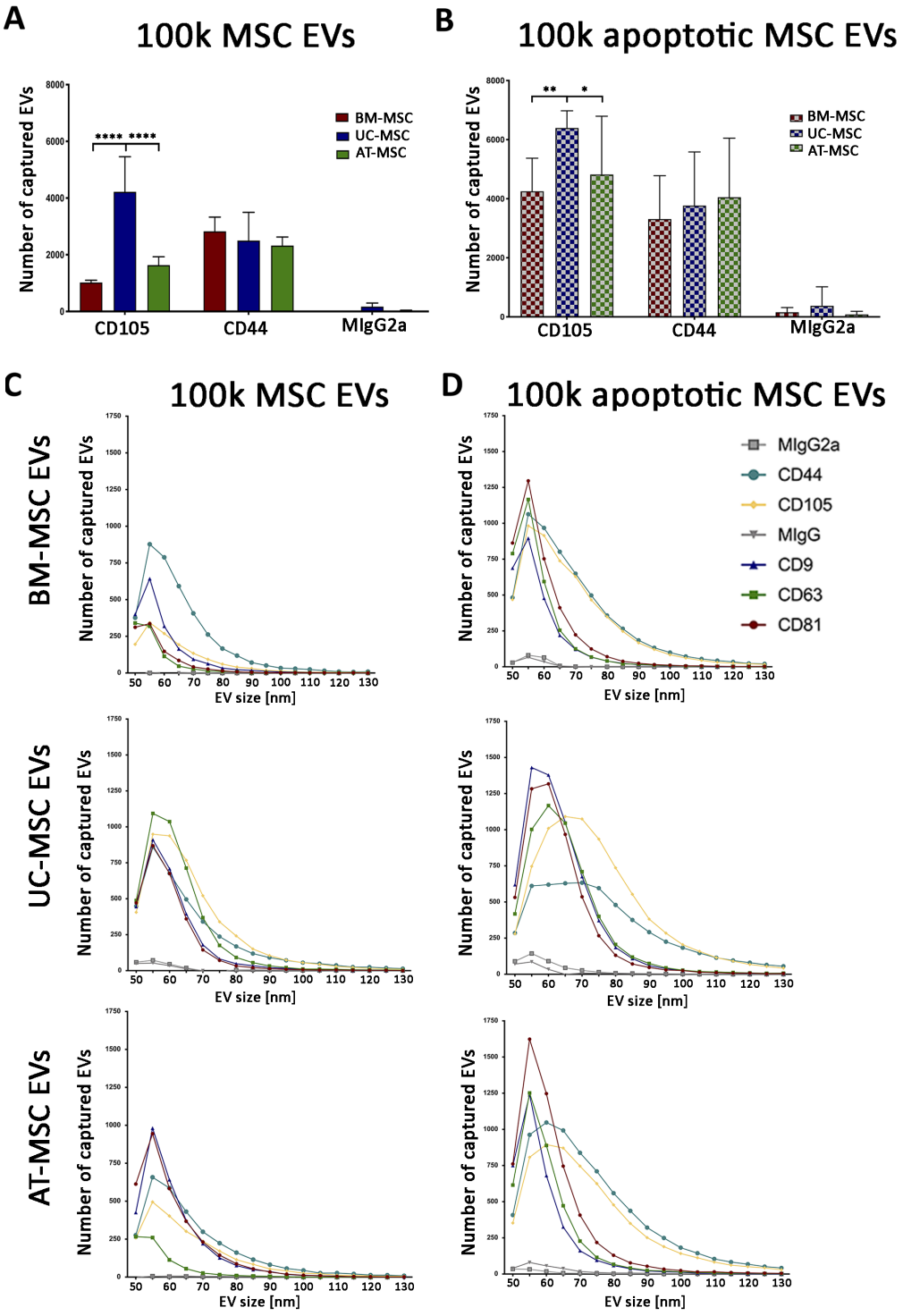

Figure 9: ExoView mesenchymal marker analysis of 100k of naïve and apoptotic MSC EVs. (A, B) Histograms showing the number of captured EVs for mesenchymal markers (CD44, CD105) and negative control for 100k MSC EVs (A) and 100k apoptotic MSC EVs (B). Data are mean ± SD of three different experiments. A p value < 0.05 was considered significant (*<0.05, **<0.001, ***<0.001, ****<0.0001). (C, D) Size of naïve (C) and apoptotic (D) 100k MSC EVs from BM-MSC EVs, UC-MSC EVs and AT-MSC EVs.

Moreover, by MACSPlex exosome kit, all EVs were negative for CD14, CD19, CD31 and CD45, as the originating cells (data not shown). Interestingly, the 100k fractions were constantly negative for immunological markers, selectively expressed by the 10k EVs (Fig. 10 A-D). In particular, the fraction enriched for 10k EVs both in naïve and apoptotic conditions was selectively expressing HLA-class I and CD40 co-stimulatory molecule. Moreover, tissue factor (TF), known to be involved in platelet activation, was expressed by 10k EVs of AT- and UC-MSC EVs, and not from those of BM-MSC EVs (Fig. 10 B, D).

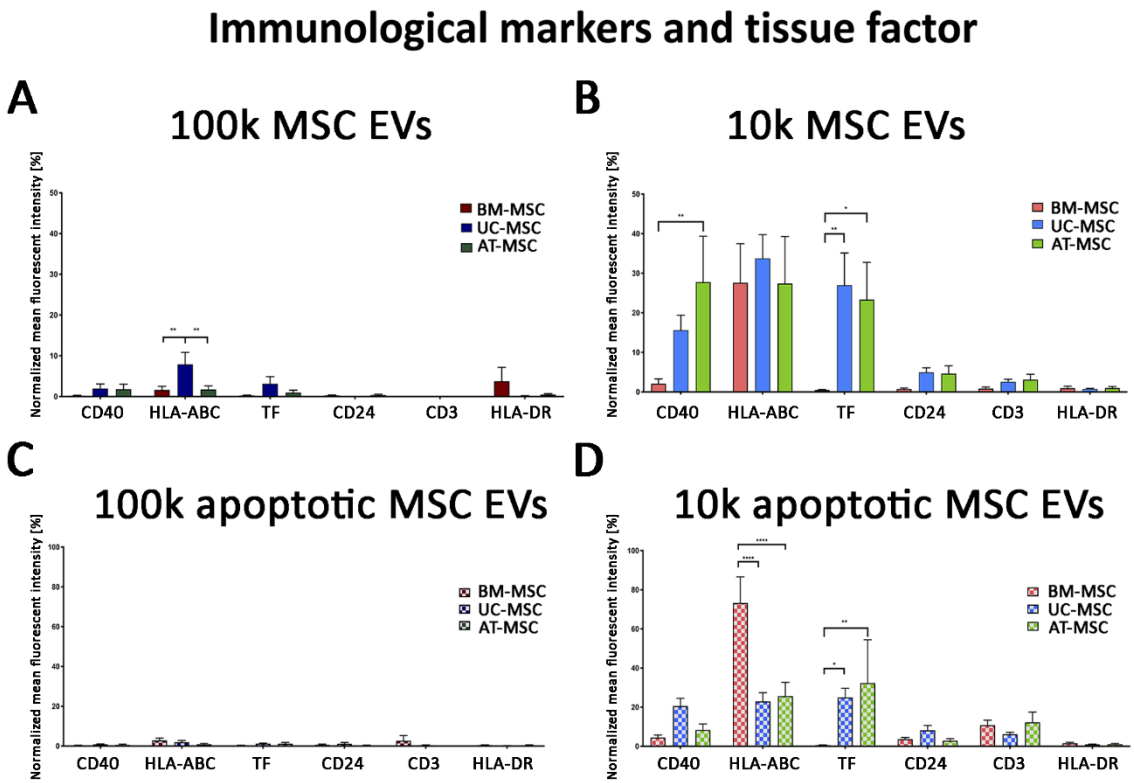

Figure 10: MACSPlex immunological marker analysis of 100k and 10k MSC EVs of naïve and apoptotic MSCs. (A-D) Histograms represent normalized fluorescence intensity of immunity markers (CD40, HLA-ABC, CD24, CD3 and HLA-DR) and tissue factor (TF) for 100k MSC EVs (A, C) and 10k MSC EVs (B, D) isolated from naïve (A, B) and apoptotic (C, D) MSCs. BM-MSC EVs, UC-MSC EVs and AT-MSC EVs were compared. Data are expressed as mean fluorescence intensity normalized to the mean fluorescence intensity of tetraspanins± SD of three different experiments. A p value < 0.05 was considered significant (*<0.05, **<0.001, ***<0.001, ****<0.0001).

Discussion

Small MSC EVs appear as the most promising EV type for therapeutic application, and the information on the surface marker expression characterising the different MSC sources and fractions is of importance. This study presents quantitative analysis of surface expression profile of tetraspanins, at a single EV level, showing variable tetraspanin coexpression in all EV fractions and sources by super resolution microscopy. Moreover, using bead-based cytofluorimetric analysis and chip-based arrays, tetraspanins as well as other clinically relevant markers (mesenchymal, immunological and pro-coagulative markers) were compared in MSC EVs from three sources in naïve or apoptotic condition. The results highlight a similar characterization profile of MSC EVs from the different MSC sources, with variable but consistent tetraspanin expression. Moreover, we observed an increased expression of mesenchymal surface markers and the restricted expression of HLA-class I, the co-stimulatory molecule CD40 and tissue factor by 10k MSC EVs, in respect to 100k MSC EVs. Finally, apoptotic conditions only modified the number, but not the characterization profile, of MSC EVs.

Thanks to an extensive effort of the EV community, the minimal criteria for EV characterization have been set (Théry et al. 2018). The analysis of the EV preparation includes a bulk analysis of protein expression demonstrating the EV identity and purity together with qualitative and quantitative analysis using a particle counter and electron microscopy (Van Deun et al. 2017). In recent years, the development of new nanotechnological instruments may allow the assessment of EV identity at a single EV level, using affinity-based chips, super resolution microscopy and high-resolution flow cytometry.

We here compared different orthogonal methods to provide a single EV analysis of 100k and 10k MSC EVs, highlighting their potential contribution and utility for the 100k MSC EVs characterization. The analysis of the EV size appeared discordant between the commonly used nanoparticle tracking analysis and the other methods. In fact, nanoparticle tracking analysis clearly showed a differential profile of 100k and 10k EVs, but the mean size of the 100k fraction was higher than that detected with other quantitative methods, as previously described (Bruno et al. 2017). This could be due to phenomena of EV aggregation, or to the influence of both temperature and Brownian motion incorporated in the nanoparticle tracking method of EV characterization. In addition, particle size using this method can result in non-consistent data; similar analyses were reported with a difference of 15–50% in the size (Rohde, Pachler, and Gimona 2019).

Electron microscopy analysis clearly showed that the 100k MSC EVs and 10k MSC EVs had distinct size. Interestingly, this observation was in line with that obtained by the specific analysis of tetraspanin expressing EVs, acquired with super-resolution microscopy on more than 10,000 analysed fresh unfixed EVs. In addition, quantitative single-vesicle imaging by super-resolution microscopy revealed heterogeneous pattern of tetraspanin expressions (single, double and triple) in variable proportions in 100k and 10k MSC EVs. Recently, a single-vesicle imaging and co-localization analysis of tetraspanins was investigated in EVs derived from HEK397, breast cancer and melanoma cell line, showing distinct fractions of single, double or triple co-expressing EVs, depending on the analysed EV type (Han et al. 2021). This is consistent with the observation that CD9 and CD81 positive EVs did not correlate with distinct EV populations using size-based EV separation technique (Jeong et al. 2018). Another relevant feature was the patchy distribution of tetraspanins on the EV surface, mainly characteristic of 10k EVs. Indeed, tetraspanins are known to homodimerize and form large complexes (Kovalenko et al. 2004). This may suggest the ability of tetraspanins on EV surface to move within the lipidic membrane, as described for the cell membrane, with capping after antibody binding (Hadjiargyrou et al. 1996).

Different MSC sources can be identified for clinical application of deriving EVs, the BM-MSC EVs being the first and most used in clinical trials. However, EVs from adipose tissue and umbilical cord might display advantages for easier cell isolation from adipose tissue, reduced impact of donor diseases or enhanced potency for umbilical cord (Kern et al. 2006). We therefore compared 100k and 10k EVs from MSCs cultured in completely identical culture conditions (media and serum, expansion number and passages) for the expression of clinically relevant markers using a standard semiquantitative cytofluorimetric assay commonly used to assess MSC EV profile (Wiklander et al. 2018). Interestingly, mesenchymal markers were present in both 100k MSC EVs and 10k MSC EVs, but with higher expression in the apoptotic EV fractions. At variance, HLA class I, co-stimulatory molecule and tissue factor expression were selectively expressed on 10k MSC EVs. These data suggest that the 100k MSC EV fractions have a good safety for clinical application, avoiding possible development of anti-HLA antibodies and rejection. Moreover, 10k EVs from AT- or UC-MSCs also showed the expression of tissue factor. This is in line with the increased coagulative capacity of 10k than of the 100k MSC EV fractions previously reported (Gamperl et al. 2016). Moreover, 10k BM-MSC EVs appeared to display the lowest expression of tissue factor, in analogy with reports

showing higher thrombogenic activity of UC- or AT-MSCs in respect to BM-MSC EVs (Chance et al. 2019; Silachev et al. 2019).

Finally, in the present study we also compared naïve MSC EVs and apoptotic MSC EVs from the different MSC sources. Indeed, apoptotic EVs are considered to display peculiar functions, and are now considered an additional but distinct MSC product with potent immunoregulatory ability (Caruso and Poon 2018). The EVs were released by apoptotic cells after Fas receptor triggering (Adachi et al. 2003; Wang et al. 2017), and apoptosis confirmed by the detection of apoptotic bodies and by expression of Phosphatidylserin (Leventis and Grinstein 2010) and Annexin V by apoptotic EVs (Atkin-Smith et al. 2015). The most relevant feature observed was the increase in number of both 100k and 10k MSC EVs released from all MSC types under apoptotic conditions. Moreover, apoptotic EVs expressed higher tetraspanin levels and mesenchymal markers in respect to the normal counterpart, as evaluated by ExoView and MACSPlex analysis respectively.

In conclusion, our results show that the characterization profile of MSC EV fractions is consistent among different MSC sources, with an increased number of EVs released under apoptotic condition. Moreover, the 100k MSC EV population display a safer profile than the 10k MSC EV population for immunological and pro-coagulative marker expression. Finally, our study identified advantages of the different EV analytical techniques for specific applications. In particular, super-resolution microscopy was useful to characterize a large number of EVs at a single EV level, whereas ExoView analysis allowed an easy quantitative comparison of marker expression among fractions of different origins and conditions. In addition, bead-based cytofluorimetric analysis appeared of utility for its large variety of markers of clinical applicability, although can only provide semiquantitative results. These results suggest that quantitative EV analysis methods are useful and reliable to be applied for the characterization of MSC EV fractions.

Funding

This project has received funding from the European Union's Horizon 2020 research and innovation programme under the Marie Skłodowska-Curie Grant agreement No. 813839.

Acknowledgments

The authors thank Natalia Gebara for her support with preparinng and analysing the experiments; Eleonora Scaccia, Erika Erika, Francesco Amadeo and Sandra Calcat for isolating and providing MSCs; Pradeep Kumar for help with super-resolution microscopy acquisition and analysis. The authors also thank prof. Marco Sassoe Pognetto of the Department of Neurosciences of the University of Turin for the use of the electron microscopy facility.

Conflicts of Interest

The authors declare no conflict of interest.

Bibliography

Adachi, Keiko, Mitsuhiko Osaki, Satoru Kase, Ami Takeda, and Hisao Ito. 2003. "Anti-Fas Antibody-Induced Apoptosis and Its Signal Transduction in Human Gastric Carcinoma Cell Lines." *International Journal of Oncology*, no. 20: 713–19. https://doi.org/10.3892/ijo.23.3.713.

Aliotta, Jason M., Mandy Pereira, Sicheng Wen, Mark S. Dooner, Michael Del Tatto, Elaine Papa, Laura R. Goldberg, et al. 2016. "Exosomes Induce and Reverse Monocrotaline-Induced Pulmonary Hypertension in Mice." *Cardiovascular Research* 110 (3): 319–30. https://doi.org/10.1093/cvr/cvw054.

Atkin-Smith, Georgia K., Rochelle Tixeira, Stephanie Paone, Suresh Mathivanan, Christine Collins, Michael Liem, Katharine J. Goodall, Kodi S. Ravichandran, Mark D. Hulett, and Ivan K.H. Poon. 2015. "A Novel Mechanism of Generating Extracellular Vesicles during Apoptosis via a Beads-on-a-String Membrane Structure." *Nature Communications* 6 (May). https://doi.org/10.1038/ncomms8439.

Bruno, Stefania, Marta Tapparo, Federica Collino, Giulia Chiabotto, Maria Chiara Deregibus, Rafael Soares Lindoso, Francesco Neri, et al. 2017. "Renal Regenerative Potential of Different Extracellular Vesicle Populations Derived from Bone Marrow Mesenchymal Stromal Cells." *Tissue Engineering - Part A* 23 (21–22): 1262–73. https://doi.org/10.1089/ten.tea.2017.0069.

Bussolati, Benedetta, Peter Hauser, Raquel Carvalhosa, and Giovanni Camussi. 2009. "Contribution of Stem Cells to Kidney Repair." *Current Stem Cell Research & Therapy* 4 (1): 2–8. https://doi.org/10.2174/157488809787169129.

Caruso, Sarah, and Ivan K.H. Poon. 2018. "Apoptotic Cell-Derived Extracellular Vesicles: More than Just Debris." *Frontiers in Immunology* 9 (JUN). https://doi.org/10.3389/fimmu.2018.01486.

Chance, Tiffani C., Christopher R. Rathbone, Robin M. Kamucheka, Grantham C. Peltier, Andrew P. Cap, and James A. Bynum. 2019. "The Effects of Cell Type and Culture Condition on the Procoagulant Activity of Human Mesenchymal Stromal Cell-Derived Extracellular Vesicles." *The Journal of Trauma and Acute Care Surgery* 87 (1S Suppl 1): S74–82. https://doi.org/10.1097/TA.0000000000002225.

Chargaff, E., and R. West. 1946. "The Biological Significance of the Thromboplastic Protein of Blood." *The Journal of Biological Chemistry* 166 (1): 189–97. https://doi.org/10.1016/s0021-9258(17)34997-9.

Crescitelli, Rossella, Cecilia Lässer, Tamas G. Szabó, Agnes Kittel, Maria Eldh, Irma

Dianzani, Edit I. Buzás, and Jan Lötvall. 2013. "Distinct RNA Profiles in Subpopulations of Extracellular Vesicles: Apoptotic Bodies, Microvesicles and Exosomes." *Journal of Extracellular Vesicles* 2 (1): 1–10. https://doi.org/10.3402/jev.v2i0.20677.

Deun, Jan Van, Pieter Mestdagh, Patrizia Agostinis, Özden Akay, Sushma Anand, Jasper Anckaert, Zoraida Andreu Martinez, et al. 2017. "EV-TRACK: Transparent Reporting and Centralizing Knowledge in Extracellular Vesicle Research." *Nature Methods* 14 (3): 228–32. https://doi.org/10.1038/nmeth.4185.

Flemming, Antoinette, Katharina Schallmoser, Dirk Strunk, Meaghan Stolk, Hans Dieter Volk, and Martina Seifert. 2011. "Immunomodulative Efficacy of Bone Marrow-Derived Mesenchymal Stem Cells Cultured in Human Platelet Lysate." *Journal of Clinical Immunology* 31 (6): 1143–56. https://doi.org/10.1007/s10875-011-9581-z.

Gamperl, Hans, Corinna Plattfaut, Annika Freund, Tabea Quecke, Friederike Theophil, and Frank Gieseler. 2016. "Extracellular Vesicles from Malignant Effusions Induce Tumor Cell Migration: Inhibitory Effect of LMWH Tinzaparin." *Cell Biology International* 40 (10): 1050–61. https://doi.org/10.1002/cbin.10645.

Giebel, Bernd, Lambros Kordelas, and Verena Börger. 2017. "Clinical Potential of Mesenchymal Stem/Stromal Cell-Derived Extracellular Vesicles." *Stem Cell Investigation* 4 (10): 1–12. https://doi.org/10.21037/sci.2017.09.06.

Gimona, Mario, Maria Felice Brizzi, Andre Boon Hwa Choo, Massimo Dominici, Sean M. Davidson, Johannes Grillari, Dirk M. Hermann, et al. 2021. "Critical Considerations for the Development of Potency Tests for Therapeutic Applications of Mesenchymal Stromal Cell-Derived Small Extracellular Vesicles." *Cytotherapy* 23. https://doi.org/10.1016/j.jcyt.2021.01.001.

Hadjiargyrou, Michael, Zaven Kaprielian, Nobuo Kato, and Paul H. Patterson. 1996. "Association of the Tetraspan Protein CD9 with Integrins on the Surface of S-16 Schwann Cells." *Journal of Neurochemistry* 67 (6): 2505–13. https://doi.org/10.1046/j.1471-4159.1996.67062505.x.

Han, Chungmin, Hyejin Kang, Johan Yi, Minsu Kang, Hyunjin Lee, Yongmin Kwon, Jaehun Jung, Jingeol Lee, and Jaesung Park. 2021. "Single-Vesicle Imaging and Co-Localization Analysis for Tetraspanin Profiling of Individual Extracellular Vesicles." *Journal of Extracellular Vesicles* 10 (3). https://doi.org/10.1002/jev2.12047.

Humphreys, Benjamin D., and Joseph V. Bonventre. 2008. "Mesenchymal Stem Cells in Acute Kidney Injury." *Annual Review of Medicine* 59: 311–25.

https://doi.org/10.1146/annurev.med.59.061506.154239.

Jeong, Hwapyeong, Chungmin Han, Siwoo Cho, Yogesh Gianchandani, and Jaesung Park. 2018. "Analysis of Extracellular Vesicles Using Coffee Ring." *ACS Applied Materials and Interfaces* 10 (27): 22877–82. https://doi.org/10.1021/acsami.8b05793.

Kern, Susanne, Hermann Eichler, Johannes Stoeve, Harald Klüter, and Karen Bieback. 2006. "Comparative Analysis of Mesenchymal Stem Cells from Bone Marrow, Umbilical Cord Blood, or Adipose Tissue." *Stem Cells* 24 (5): 1294–1301. https://doi.org/10.1634/stemcells.2005-0342.

Kovalenko, Oleg V., Xiuwei Yang, Tatiana V. Kolesnikova, and Martin E. Hemler. 2004. "Evidence for Specific Tetraspanin Homodimers: Inhibition of Palmitoylation Makes Cysteine Residues Available for Cross-Linking." *Biochemical Journal* 377 (2): 407–17. https://doi.org/10.1042/BJ20031037.

Kowal, Joanna, Guillaume Arras, Marina Colombo, Mabel Jouve, Jakob Paul Morath, Bjarke Primdal-Bengtson, Florent Dingli, Damarys Loew, Mercedes Tkach, and Clotilde Théry. 2016. "Proteomic Comparison Defines Novel Markers to Characterize Heterogeneous Populations of Extracellular Vesicle Subtypes." *Proceedings of the National Academy of Sciences of the United States of America* 113 (8): E968–77. https://doi.org/10.1073/pnas.1521230113.

Lener, Thomas, Mario Gimona, Ludwig Aigner, Verena Börger, Edit Buzas, Giovanni Camussi, Nathalie Chaput, et al. 2015. "Applying Extracellular Vesicles Based Therapeutics in Clinical Trials - An ISEV Position Paper." *Journal of Extracellular Vesicles* 4 (1). https://doi.org/10.3402/jev.v4.30087.

Leventis, Peter A., and Sergio Grinstein. 2010. "The Distribution and Function of Phosphatidylserine in Cellular Membranes." *Annual Review of Biophysics* 39 (1): 407–27. https://doi.org/10.1146/annurev.biophys.093008.131234.

Mobarrez, Fariborz, Carolina Sjövik, Anne Soop, Lars Hållström, Claes Frostell, David S. Pisetsky, and Håkan Wallén. 2015. "CD40L Expression in Plasma of Volunteers Following LPS Administration: A Comparison between Assay of CD40L on Platelet Microvesicles and Soluble CD40L." *Platelets* 26 (5): 486–90. https://doi.org/10.3109/09537104.2014.932339.

Park, Kyong Su, Elga Bandeira, Ganesh V. Shelke, Cecilia Lässer, and Jan Lötvall. 2019. "Enhancement of Therapeutic Potential of Mesenchymal Stem Cell-Derived Extracellular Vesicles." *Stem Cell Research and Therapy* 10 (1): 1–15. https://doi.org/10.1186/s13287-019-1398-3.

Rohde, Eva, Karin Pachler, and Mario Gimona. 2019. "Manufacturing and Characterization of Extracellular Vesicles from Umbilical Cord–Derived Mesenchymal Stromal Cells for Clinical Testing." *Cytotherapy* 21 (6): 581–92. https://doi.org/10.1016/j.jcyt.2018.12.006.

Silachev, Denis, Kirill Goryunov, Margarita Shpilyuk, Olga Beznoschenko, Natalya Morozova, Elizaveta Kraevaya, Vasily Popkov, et al. 2019. "Effect of MSCs and MSC-Derived Extracellular Vesicles on Human Blood Coagulation." *Cells* 8 (3): 258. https://doi.org/10.3390/cells8030258.

Théry, Clotilde, Kenneth W Witwer, Elena Aikawa, Maria Jose Alcaraz, Johnathon D Anderson, Ramaroson Andriantsitohaina, Anna Antoniou, et al. 2018. "Minimal Information for Studies of Extracellular Vesicles 2018 (MISEV2018): A Position Statement of the International Society for Extracellular Vesicles and Update of the MISEV2014 Guidelines." *Journal of Extracellular Vesicles* 7 (1): 1535750. https://doi.org/10.1080/20013078.2018.1535750.

Tixeira, Rochelle, Sarah Caruso, Stephanie Paone, Amy A. Baxter, Georgia K. Atkin-Smith, Mark D. Hulett, and Ivan K.H. Poon. 2017. "Defining the Morphologic Features and Products of Cell Disassembly during Apoptosis." *Apoptosis* 22 (3): 475–77. https://doi.org/10.1007/s10495-017-1345-7.

Wang, Yu, Chunhui Xia, Yanxin Lv, Chengjun Li, Qingbu Mei, Hongmei Li, Haijun Wang, and Shuang Li. 2017. "Crosstalk Influence between P38MAPK and Autophagy on Mitochondria-Mediated Apoptosis Induced by Anti-Fas Antibody/Actinomycin D in Human Hepatoma Bel-7402 Cells." *Molecules* 22 (10). https://doi.org/10.3390/molecules22101705.

Wen, Sicheng, Mark Dooner, Yan Cheng1, Elaine Papa, Michael Del Tatto, Mandy Pereira, Yanhui Deng, et al. 2016. "Mesenchymal Stromal Cell Derived Extracellular Vesicles Rescue Radiation Damage to Murine Marrow Hematopoietic Cells Sicheng." *Physiology & Behavior* 176 (1): 139–48. https://doi.org/10.1038/leu.2016.107.Mesenchymal.

Wiklander, Oscar P.B., R. Beklem Bostancioglu, Joshua A. Welsh, Antje M. Zickler, Florian Murke, Giulia Corso, Ulrika Felldin, et al. 2018. "Systematic Methodological Evaluation of a Multiplex Bead-Based Flow Cytometry Assay for Detection of Extracellular Vesicle Surface Signatures." *Frontiers in Immunology* 9 (JUN). https://doi.org/10.3389/fimmu.2018.01326.

Willms, Eduard, Henrik J. Johansson, Imre Mäger, Yi Lee, K. Emelie M. Blomberg, Mariam Sadik, Amr Alaarg, et al. 2016. "Cells Release Subpopulations of Exosomes with

Distinct Molecular and Biological Properties." *Scientific Reports* 6 (February): 1–12. https://doi.org/10.1038/srep22519.

Witwer, Kenneth W., Bas W.M. Van Balkom, Stefania Bruno, Andre Choo, Massimo Dominici, Mario Gimona, Andrew F. Hill, et al. 2019. "Defining Mesenchymal Stromal Cell (MSC)-Derived Small Extracellular Vesicles for Therapeutic Applications." *Journal of Extracellular Vesicles* 8 (1). https://doi.org/10.1080/20013078.2019.1609206.

Xu, Rong, David W. Greening, Alin Rai, Hong Ji, and Richard J. Simpson. 2015. "Highly-Purified Exosomes and Shed Microvesicles Isolated from the Human Colon Cancer Cell Line LIM1863 by Sequential Centrifugal Ultrafiltration Are Biochemically and Functionally Distinct." *Methods* 87: 11–25. https://doi.org/10.1016/j.ymeth.2015.04.008.

Yáñez-Mó, María, Pia R-M Siljander, Zoraida Andreu, Apolonija Bedina Zavec, Francesc E Borràs, Edit I Buzas, Krisztina Buzas, et al. 2015. "Biological Properties of Extracellular Vesicles and Their Physiological Functions." *Journal of Extracellular Vesicles* 4 (May): 27066. https://doi.org/10.3402/jev.v4.27066.